Biominerals

Dissolution at the Nanoscale: Self-Preservation of Biominerals**

*Ruikang Tang, Lijun Wang, Christine A. Orme, Tammy Bonstein, Peter J. Bush, and George H. Nancollas**

Despite the complicated hierarchical structures of natural materials such as shells, bones, and teeth, their basic building blocks are generally in the nanometer size range[1–6] to ensure optimum physical and biological functions.[5–7] Herein we reveal that this nanostructural optimization also confers on the biomaterials remarkable characteristics of dynamic preservation. Generally, dissolution of minerals is regarded as a spontaneous reaction in which all the solid phase can be dissolved in undersaturated solutions. However, it has been found that demineralization reactions actually involve particle-size-dependent critical conditions of energetic control at the molecular level.[8–10] It suggests that the dissolution of crystallites may be inhibited or even suppressed when their sizes fall into the same range as that of a certain critical value—always at a nanoscale level. Therefore, these nanostructured biominerals can be resistant to dissolution on account of their sizes and can remain relatively stable in the biological milieux even though the latter may be undersaturated. This new lesson from nature enriches our understanding of nanostructured materials and biological demineralization.

Enamel layers at tooth surfaces are among the hardest biological tissues.[4,11,12] In this Communication, enamel is selected as an example in the context of nanodemineralization since it is highly mineralized and exhibits features that are close to pure synthetic apatites with about 97% mineral phase and about 3% water and organic matrix.[11–13] Scanning electron micrographs (SEM) of enamel surfaces prior to significant dissolution (Figure 1a) show the well-organized

[*] Dr. R. Tang, Dr. L. Wang, Prof. G. H. Nancollas
Department of Chemistry
University at Buffalo
The State University of New York
Buffalo, NY 14260 (USA)
Fax: (+1) 716-645-6947
E-mail: ghn@buffalo.edu
Dr. C. A. Orme
Department of Chemistry and Materials Sciences
Lawrence Livermore National Laboratory
Livermore, California 94550 (USA)
Dr. T. Bonstein, P. J. Bush
Instrumentation Center, School of Dental Medicine
University at Buffalo
The State University of New York
Buffalo, New York 14260 (USA)

[**] This work was supported by the National Institutes of Health (NIDCR grant number DE03223). We thank Drs. J. De Yoreo and D. White for helpful discussions and G. Jones for assistance with the XPS studies

 DOI: 10.1002/ange.200353652

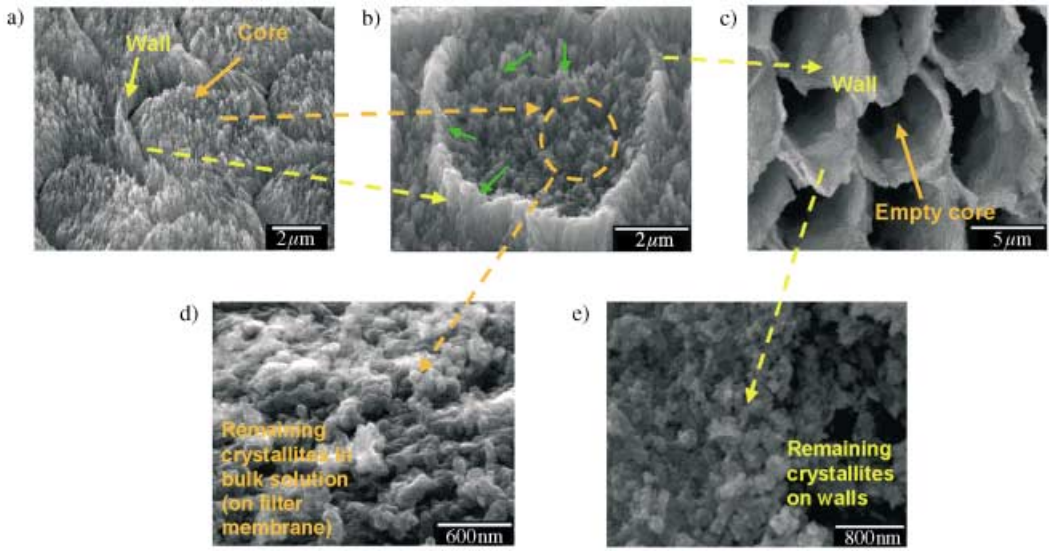

Figure 1. Demineralization of dental enamel: yellow and orange labels mark the dissolution of the walls and cores, respectively, thus showing that they undergo similar dissolution processes. a) Well-organized rod structures on mature human enamel surfaces: both the walls and cores are composed of numerous needlelike apatites that have the same chemical and physical properties. However, the crystallites in the cores are oriented perpendicular to the enamel surface while those on the walls are inclined by 10–40°. b) During dissolution, crystallites becomes smaller and nanosized apatite particles (shown by green arrows; see also Figure 2) are formed on both walls and cores. c) After 7 days of dissolution, the cores are emptied but the walls remain. d) Nanosized apatite particles collected from the bulk solution by filtration (Nucleopore N003 filter membrane) at the end of dissolution experiment. These particles have escaped from cores and walls (Figure 1 b) but are resistant to further dissolution even though the solution is undersaturated. e) SEM of the wall at higher magnification; nanosized apatite residues, retained on the wall surfaces, are kinetically protected against further dissolution.

rodlike structures. Previous[4,12] studies and our current results of in situ electron dispersive spectroscopy (EDS), X-ray diffraction (XRD), X-ray photoelectron spectroscopy (XPS) and infrared (IR) indicate identical chemical and crystallographic properties of the minerals in cores and on walls, both being composed of numerous needlelike inorganic apatites, but the crystallites in the cores are oriented perpendicular to the enamel surface, while those on the walls are inclined by 10–40°. During enamel maturation, it has been suggested that the proteins (mainly amelogenins) that induce/control the crystallization of apatite are almost completely degraded or removed.[4,14,15]

Under physiological conditions of temperature (37 °C, $T=$ 310 K) and ionic strength (0.15 M), it is found that demineralization of enamel surfaces will only take place at relatively high undersaturations ($S<0.4$, S is undersaturation, see Experimental Section) and at lower pH (<5.5); otherwise, no dissolution can be experimentally detected. In this study, the demineralization of enamel has been investigated over an extended experimental period of 1–10 day(s) at $S=0.10$ and pH 4.5 by using a nanomolar-sensitive constant-composition (CC) technique[16] combined with in situ atomic force microscopy (AFM). It is found that apatite crystallites both in the cores and on the walls undergo similar demineralization processes (Figure 1). Figure 1 b shows walls and cores at an intermediate stage during the dissolution reaction, in which the nanosized apatite particles ($\approx$100 nm) that result from dissolution can be seen on both surfaces (Figure 2). However, further dissolution of these nanosized particles was suppressed: 1) Those from cores were released directly into the solution by fluid diffusion flux, thus resulting in empty cores (Figure 1 c); these particles were stable against dissolution in the bulk solution (Figure 1 d; it should be noted that they are of similar size to those in Figure 1 b, $\approx$80–100 nm). 2) The small particles from the walls also did not dissolve but they adhered to the wall framework. It has been shown that almost all of the organic components in enamel are found in the

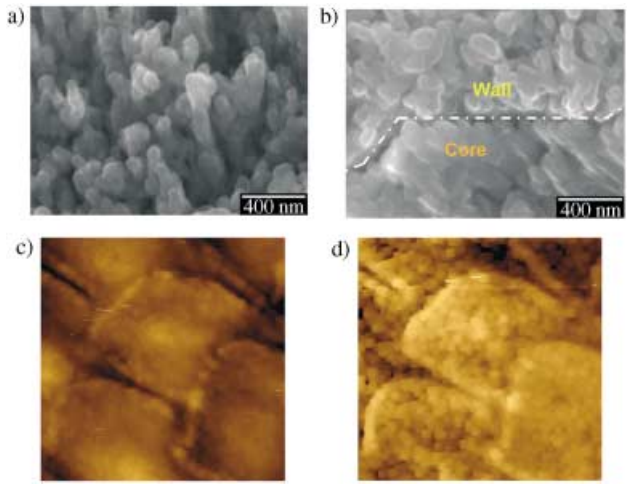

Figure 2. Enlargement of Figure 1 b, both the core (a) and wall surfaces (b) are covered by numerous apatite particles of similar nanosize following demineralization. This phenomenon is also observed and confirmed by in situ AFM studies, c) and d) show the enamel surfaces in solution near the beginning of the dissolution experiment and after 4 h of reaction, respectively. The formation of the nano particles (2 d, 100–200 nm) is observed in this real time experiment. The AFM image scales are 8×8 μm.

walls,[17] which remain intact at the end of the dissolution experiments (Figure 1c). High magnification SEM confirms that the remaining wall surfaces are actually covered by numerous small crystallites 100 ± 20 nm in size (Figure 1e). This demineralization of enamel surfaces was also confirmed by in situ AFM studies (Figure 2c and d); the formation and release of the nanoparticles during the dissolution reaction were observed in real time. All the results of in situ EDS, XRD, XPS, and IR studies indicate that these residual crystallites are apatitic phases similar to those prior to demineralization. The apatitic residues of the demineralization reactions, both from walls and cores, have the same size distribution range (Figures 1d,e and 2) and are stabilized against further dissolution in the undersaturated aqueous solution.

To exclude the influence of complicating biological factors such as the possible presence of organic matrix components, CC dissolution studies have also been made by using synthetic hydroxyapatite ($Ca_5(PO_4)_3OH$) samples of high purity (>99.4%) with needlelike morphology (400–600 nm length, 60–100 nm width). Similar reproducible self-inhibited dissolution was observed with these nanosized crystallites. At a high undersaturation ($S = 0.02$), they undergo rapid dissolution ($4.0 \pm 0.3 \times 10^{-6}$ mol m^{-2} min^{-1}) and almost all of solid phase is dissolved in less than 3 h. However, at lower undersaturation, the rates decrease during the reaction; at $S = 0.580$, the initial rate, $3.2 \pm 0.2 \times 10^{-7}$, decreases to $1.6 \pm 0.1 \times 10^{-7}$ and $0.8 \pm 0.1 \times 10^{-7}$ mol m^{-2} min^{-1} at 50 min and 90 min, respectively. The CC dissolution curves reach plateaux prior to complete dissolution (Figure 3a), thus indicating the creation of metastable states in which the reaction is effectively terminated even though the apatite crystallites remain in contact with the undersaturated solutions. This result is similar to the observations made during enamel demineralization. The residual crystallites are confirmed to be of the same chemical compositions as the initial seed crystals. At $S = 0.315$, 90% (by mass) of the seed crystals are dissolved and this decreases markedly with deceasing undersaturation; at an undersaturation of 0.580, only a relatively small fraction (38%) of the apatite crystallites undergo dissolution before the reaction is effectively stopped or reduced to a very low rate. No immediate CC dissolution of the seed crystallites could be detected at lower undersaturations (e.g. $S = 0.828$, Figure 3).

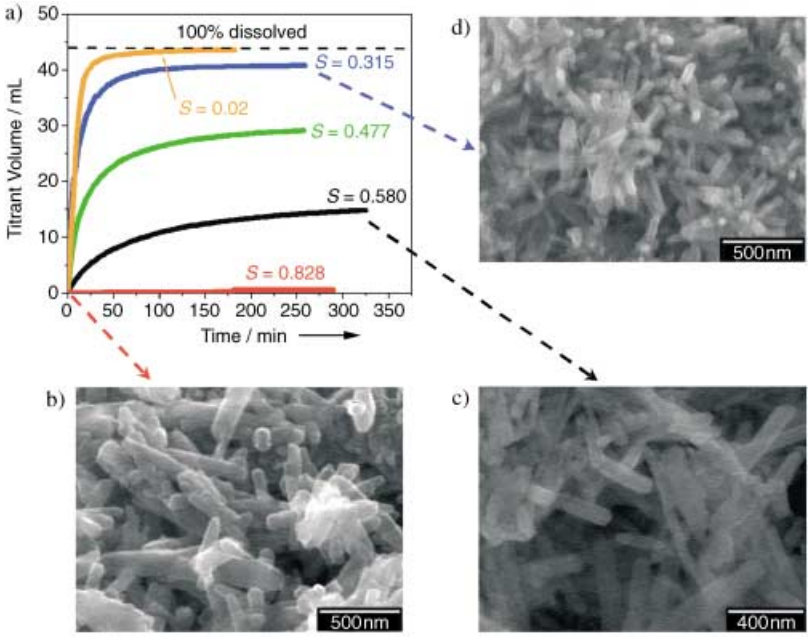

Figure 3. In vitro CC dissolution of synthetic hydroxyapatite. a) CC plots of titrant volume against time at different undersaturations. The red lines indicate the titrant volumes for full dissolution of the added seeds. Only at very high undersaturation ($S = 0.02$), does the dissolution go to completion. The dissolution rates decrease with time and eventually, only a fraction of the added seeds undergo dissolution before the rates approach zero. Near equilibrium ($S = 0.828$) no dissolution can be detected in the undersaturated solutions. For the smaller hydroxyapatite seeds (length, 200–300 nm and width, 50–80 nm), no CC dissolution can be detected at an even higher undersaturation of $S \geq 0.720$. This value for enamel is $S \geq 0.4$, showing the much less extensive dissolution. b) SEM of seed crystals and c crystallites remaining at the end of dissolution experiments at $S = 0.580$ and d) $S = 0.315$. The results are similar to those for enamel dissolution.

Clearly, this dissolution termination is a kinetic phenomenon and cannot be attributed to reaction retardation as a result of surface modification by additives. However, it can be explained in terms of a dissolution model that incorporates particle size considerations. It has been suggested, and confirmed by experiment, that demineralization of sparingly soluble salts such as apatite is generally initiated and accompanied by the formation and development of pits on the crystal surfaces and that the dissolution rates are also determined by the pit densities and spreading velocities.[8–10,18,19] Analogous to the formation of two dimensional nuclei/hillocks for crystal growth, in dissolution the rate of step movement from a pit of radius r can be obtained from treatments similar to the model of Burton, Cabrera, and Frank,[8–10,20,21]

In Equation (1), r^*, the critical radius for the formation of a two-dimensional pit/dissolution step, is given by Equation (2)[20,21]

$$R(r) = R_\infty \left[1 - \frac{e^{(1-S)r^*/r - 1}}{e^{1-S} - 1}\right] \approx R_\infty \left(1 - \frac{r^*}{r}\right) \quad (1)$$

$$r^* = \frac{\gamma_{SL}\,\Omega}{|\Delta g|} \quad \text{and} \quad \Delta G = k\,T \ln S \quad (2)$$

in which, γ_{SL} is interfacial tension, k, the Boltzmann constant, Ω, the area occupied by each dissolution unit and ΔG, the change of the Gibbs free energy for dissolution. It has been shown that only pits larger than r^*, which provide the active dissolution sites, contribute to the reaction. In Equation (1), R_∞ is the velocity of dissolution steps at $r \rightarrow \infty$. It follows that when r is closer to r^*, its dissolution rate decreases and approaches zero when $r \rightarrow r^*$. When the dimensions of the crystallites (l) are of the same order as r^* (l is less than $20\,r^*$), it can be assumed that the formation of active pits becomes difficult on such a small crystal faces (e.g. formation of new pits with radius r^* on surfaces $2–5\,r^*$ in size) and their enlargement is strongly inhibited by the limitation of pit/crystal size (the pit sizes, r, are confined by crystallite size, l).

With decreasing active pit densities (which always decrease during dissolution,[8,19] especially when $l \rightarrow r^*$) and pit sizes ($r \propto l$), dissolution is retarded or even undetectable by CC if etch pits cannot grow to values larger than r^*. This is consistent with the CC dissolution results, which show that for crystallite sizes approaching the critical values, the rates (slopes of the CC curves in Figure 3a) decrease markedly with time despite the sustained driving force. By introducing the apatite interfacial tension, $\gamma_{SL} \approx 105\ mJ\,m^{-2}$,[22,23] and lattice structure ($a = b = 0.942$ nm, $c = 0.685$ nm), one can be estimated from Equation (1) that the value of r^* is about 20–50 nm for enamel apatites under these dissolution conditions. It is significant that the observed dissolution apatite residues in Figure 1d have very similar size distributions.

Lasaga and Luttge as well as our group have suggested that if the undersaturation (driving force for demineralization) is low (e.g $S = 0.828$ for pure hydroxyaoatite in the present work), pits will not open up and defect sites will not lead to stepwaves that form far from the localized etch pits due to the low driving force.[8,10,18] Alternately, in terms of crystallite sizes, due to the high value of r^*, active dissolution pits (250–500 nm at $S = 0.828$) are close to the crystallite size(400–600 nm). Here, we show that, although high undersaturations can induce the initial dissolution, the decreasing crystallite size also leads to the possible inhibition and even suppression of dissolution when it approaches the critical value for the active pit, r^*. The phenomena of dissolution termination and their "critical" sizes are not arbitrary; rather, these self-tuned and dissolution-insensitive effects for tiny crystallites and biomaterials such as tooth enamel occur specifically at the nanoscale.

The critical size of pits, r^*, is a function of undersaturation [Eq. (2)] and the residual apatite crystallites have sizes similar to their critical dissolution values, assuming the mean crystal size of the dissolution residues, l, is in some manner proportional to r^*. The direct relationship between the sizes of crystallites remaining after dissolution and the undersaturations can be studied by precisely controlled CC experiments and SEM (Figure 3). These confirm that the size decreases with increasing undersaturation. In terms of a 3D macroscale dissolution model for pure hydroxyapatite,[24,25] the extent of dissolution and the particle critical sizes can be estimated from the CC kinetics results.[8] From Equation (2), the ratios of the critical sizes for S of 0.580, 0.477, and 0.315 are 2.11:1.55:1.00, respectively. The results from CC dissolution kinetic experiments, 1.97:1.60:1.00, are in excellent agreement. The data are also supported by scanning electron micrographs (Figure 3) which show that although the initial seed crystals are not uniform in size, the small nanosized dissolution residues (Figure 3d) have similar size distributions (length 120 ± 20 nm, width 40 ± 10 nm). It is interesting to speculate that this marked crystallite size effect in the dissolution reactions could provide the simplest route for the formation of nanoparticles of sparingly soluble salts. Their sizes can be readily adjusted by changing the dissolution conditions.

Dissolution experiments by using smaller synthetic apatite crystallites (length, 150–250 nm, width, 20–50 nm) give similar results but the unusual dissolution phenomenon is magnified as the sizes approach the critical conditions; no dissolution can be detected even at higher undersaturation ($S = 0.720$). In contrast to conventional models (e.g., Ostwald–Freundlich) which assume smaller particles have higher solubilities and therefore dissolve faster,[26] at $S = 0.580$, the CC dissolution rates of synthetic apatite are $2.2 \pm 0.2 \times 10^{-7}\ mol\,min^{-1}\,m^{-2}$ for smaller crystallites (length, 150–250 nm and width, 20–50 nm), whereas, larger particles (length 500–600 nm and width 60–100 nm) exhibit greater dissolution rates, $3.2 \pm 0.2 \times 10^{-7}\ mol\,min^{-1}\,m^{-2}$. Our dissolution model would suggest that since the sizes of the smaller finely divided apatite crystallites are closer to the critical values, the dissolution rate is more readily self-inhibited as predicted by Equation (1) and stronger dissolution conditions must be used to induce demineralization. Similar results of size-dependent dissolution kinetics have also been shown in the case of another calcium phosphate, brushite ($CaHPO_4{\cdot}2H_2O$), which further suggest that traditional dissolution models may be applied for larger crystallites ($> 100\,r^*$).[9] Our model also explains the generally observed existence of nanoparticles in aqueous solutions: they are dynamically stable despite being thermodynamically metastable.

In a large number of biological systems, the mineral phases are composed of tiny sparingly soluble crystallites tens to thousands of nanometers in size; it appears that this is the most natural selection. It is well-known that there is a close relationship between solubility and γ_{SL}. During dissolution, some neighboring ions on the surface are replaced by water molecules to form units that escape into the bulk solution. Higher values of γ_{SL} indicate a greater difficulty in forming such an interface between the solid and aqueous phases. Thus, sparingly soluble salts in aqueous solution always have much higher interfacial free-energy values than soluble salts, thus resulting in greater values of r^* (10–100 nm). Biological minerals have sizes in this critical range and may be protected from dissolution since the reaction in the metastable region is significantly inhibited [Eq. (1)]. This accounts for the observation that the dissolution of biomineral powders is always slower than that of synthesized relatively large crystallites after normalization for specific surface area. In addition to these interesting conclusions from CC dissolution studies, it is also widely accepted that the growth of tiny apatite seeds is rarely observed at low supersaturations ($S < 4$)[27] due to extremely slow growth rates, which can again be attributed to a kinetic size effect.

For many systems in nature, nanosized mineral particles constitute the basic building blocks; typically tens to hundreds of them can be tuned to give the self-assembled mineral a remarkable "biological function and activity". However, the present results show that the biomaterials become insensitive to dissolution or even crystal growth at the nanoscale level. An excellent example is seen in studies of caries lesion formation. Enamel surfaces remain undissolved in water (pH 5.5–5.8) in spite of the undersaturation. Caries (dissolution) is only induced at localized sites where bacteria have produced acidic conditions. The mineral crystallites can be stabilized in the fluctuating physiological fluids, thus exercising a degree of self-preservation as the result of this kinetic size-effect at the nanoscale level. Furthermore, this nanodissolution behavior

of nanoparticles is also of great significance for the solvent stability and reactivity in working nanoparticle-based structures and sensors.

Experimental Section

Constant Composition (CC)

Dissolution experiments were made in magnetically stirred double-walled pyrex vessels. The undersaturated reaction solutions (200 mL) were prepared by mixing calcium chloride and potassium dihydrogen phosphate with sodium chloride to maintain the ionic strength, I, at 0.15 mol L^{-1}. The pH was adjusted to the desired value, 4.50 ± 0.01. Nitrogen, saturated with water vapor at 37 °C, was purged through the reaction solutions to exclude carbon dioxide. The dissolution reactions were initiated by the introduction of either enamel blocks ($\approx 4 \times 4 \times 0.2$ mm) or aptite seed crystallites (10.0 mg). Titrant addition was potentiometrically controlled by glass and Ag/AgCl reference electrodes. During dissolution, the electrode potential was constantly compared with a preset value and the difference, or error signal, activated a motor-driven titrant buret. Thus a constant thermodynamic dissolution driving force was maintained. Concentrations of the titrant solutions are given by Equations (3) and (4),

$$T_{NaCl} = W_{NaCl} + W_{KOH} + 6\,C_{eff} \quad (3)$$

$$T_{HCl} = 14\,C_{eff} - W_{KOH} \quad (4)$$

in which W and T are the total concentrations in the reaction solutions and titrants, respectively, and C_{eff} is the effective titrant concentration with respect to hydroxyapatite. During the reactions, slurry samples were periodically withdrawn, filtered and the solutions analyzed for calcium and phosphate. The total concentrations of calcium and phosphate remained constant to within $\pm 1.5\%$ during the experiments.

The dissolution flux rate, J, can be calculated by using Equation (5),

$$J = \frac{C_{eff}}{A_T}\frac{dV}{dt} \quad (5)$$

in which dV/dt is the gradient of the CC titrant curves and A_T is the surface area. The initial value of A_T was calculated from the specific surface area of the seeds, which was determined by BET nitrogen adsorption (30:70 N_2/He, Quantasorb II, Quantachrome); subsequent values during dissolution were estimated from a well-established 3-dimensional dissolution model for HAP.[28]

In situ atomic force microscopy: AFM images of enamel surfaces were collected in contact mode by using a Digital Instruments Nanoscope III microscope. All images were acquired in height and deflection modes by using the lowest tip force possible to reduce the tip–surface interaction. The enamel was anchored inside the fluid cell and undersaturated solution was passed through while the images were taken.

Scanning electron microscopy: Samples, under vacuum, were sputter-coated with a thin carbon deposit to provide conductivity, and then examined by using a field-emission SEM (Hitachi S-4000), typically at 20 or 30 KeV.

Supersaturation and solution speciation: The undersaturation, S, is given by Equation (6),

$$S = \left[\frac{IP}{K_s}\right]^{1/9} \quad (6)$$

in which, IP is ionic activity product and the solubility activity product of apatite, K_s, is 2.35×10^{-59}. The solution is undersaturated when $S < 1$; higher values reflect lower undersaturations. Solution speciation calculations were made by using the extended Debye–Hückel equation proposed by Davies from mass-balance expressions for total calcium and total phosphate with appropriate equilibrium constants by successive approximation for the ionic strength. Values of the dissociation constants of phosphoric acid were $K_1 = 6.22 \times 10^{-3}$, $K_2 = 6.59 \times 10^{-8}$, and $K_3 = 6.6 \times 10^{-13}$ mol L^{-1}, and the water ionic product was 2.40×10^{-14} mol^2 L^{-2}. The formation constants for the ion pairs $CaH_2PO_4^+$, $CaHPO_4$, $CaPO_4^-$, and $CaOH^+$ were taken as 28.1, 589, 1.40×10^6, and 25 L mol^{-1}, respectively.

Received: December 30, 2003
Revised: February 18, 2004 [Z53652]

Keywords: apatites · bioinorganic · biomineralization · enamel · nanostructures

[1] A. P. Alivisatos, *Science* **2000**, *289*, 736 – 737.
[2] H. Cölfen, S. Mann, *Angew. Chem.* **2003**, *115*, 2452 – 2468; *Angew. Chem. Int. Ed.* **2003**, *42*, 2350 – 2365.
[3] S. Weiner, H. D. Wagner, *Annu. Rev. Mater. Sci.* **1998**, *28*, 271 – 298.
[4] A. G. Fincham, J. Moradian-Oldak, J. P. Simmer, *J. Struct. Biol.* **1999**, *126*, 270 – 299.
[5] H. Gao, B. Ji, I. L. Jager, E. Arzt, P. Fratzl, *Proc. Natl. Acad. Sci. USA* **2003**, *100*, 5597 – 5600.
[6] S. Kamat, X. Su, R. Ballarini, A. H. Heuer, *Nature* **2000**, *405*,1036 – 1040.
[7] H. C. Lichtenegger, T. Schoberl, M. H. Bartl, H. Waite, G. D. Stucky, *Science* **2002**, *298*, 389 – 392.
[8] R. Tang, G. H. Nancollas, C. A. Orme, *J. Am. Chem. Soc.* **2001**, *123*, 5437 – 5543.
[9] R. Tang, C. A. Orme, G. H. Nancollas, *J. Phys. Chem. B* **2003**, *107*, 10653 – 10657.
[10] A. C. Lasaga, A. Luttge, *Science* **2001**, *291*, 2400 – 2404.
[11] R. Z. LeGeros, *Calcium Phosphates in Oral Biology and Medicine*, Karger, Basel, **1991**.
[12] G. Nikiforuk, *Understanding Dental Caries. Etidogy and Mechanisms Basic and Clinical Aspects*, Karger, Basel, **1985**.
[13] S. V. Dorozhkin, M. Epple, *Angew. Chem.* **2002**, *114*, 3260 – 3277; *Angew. Chem. Int. Ed.* **2002**, *41*, 3130 – 3146.
[14] A. G. Fincham, W. Luo, J. Moradian-Oldak, M. L. Paine, M. L. Snead, M. Zeichner-David, in *Development*, *Function and Evolution of Teeth* (Eds.: M. F. Teaford, M. M. Smith, M. W. J. Ferguson), Cambridge University Press, Cambridge, **2000**.
[15] J. Moradian-Oldak, *Matrix Biol.* **2001**, *20*, 293 – 305.
[16] M. B. Tomson, G. H. Nancollas, *Science* **1978**, *200*, 1059 – 1060.
[17] A. R. Pelton, R. Gronsky, D. B. Williams, *Images of Materials*, Oxford University Press, Oxford, **1991**.
[18] A. C. Lasaga, A. Luttge, *Eur. J. Mineral.* **2003**, *15*, 603 – 615.
[19] C. E. Jones, P. R. Unwin, J. V. Macpherson, *Chemphyschem* **2003**, *4*, 139 – 146.
[20] W. K. Burton, N. Cabrera, F. C. Frank, *Nature* **1949**, *163*, 398 – 399.
[21] P. Hartman, *Crystal growth: an introduction*, North-Holland, Amsterdam-London-New York-Tokyo, **1975**.
[22] W. Wu, G. H. Nancollas, *Adv. Colloid Interface Sci.* **1999**, *79*, 229 – 279.
[23] S. Koutsopoulos, P. C. Paschalakis, E. Dalas, *Langmuir* **1994**, *10*, 2423 – 2426.
[24] E. P. Paschalis, K. Wikiel, G. H. Nancollas, *J. Biomed. Mater. Res.* **1994**, *28*, 1411 – 1418.
[25] L. C. Chow, M. Markovic, S. Takagi, *J. Biomed. Mater. Res. Part B* **2003**, *65*, 245 – 251.
[26] H. Freundlich, *Colloid and Capillary Chemistry*, E. P. Dutton and Compnay, New York, **1923**.
[27] J. Christoffersen, M. R. Christoffersen, *J. Cryst. Growth* **1992**, *121*, 608 – 616.
[28] G. H. Nancollas, J. A. Budz, *J. Dent. Res.* **1990**, *69*, 1678 – 1685.

